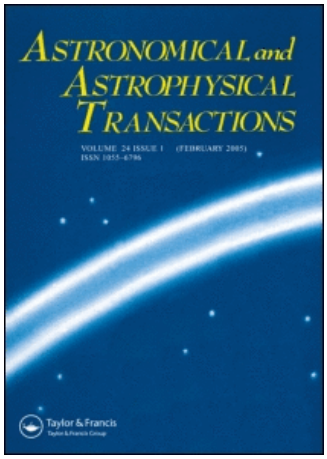

Astronomical & Astrophysical Transactions
The Journal of the Eurasian Astronomical Society
Publication details, including instructions for authors and subscription information:
http://www.informaworld.com/smpp/title~content=t713453505

HC 3 N OBSERVATIONS OF THE OUTER GALAXY DENSE CORES

L. E. Pirogov [a]; L. E. B. Johansson [b]; I. I. Zinchenko
[a] Institute of Applied Physics, Uljanova str., 46, Nizhny Novgorod, 603950, Russia.
[b] Onsala Space Observatory, S-439 92, Onsala, Sweden.

Online Publication Date: 01 February 2003
To cite this Article: Pirogov, L. E., Johansson, L. E. B. and Zinchenko, I. I. (2003) 'HC 3 N OBSERVATIONS OF THE OUTER GALAXY DENSE CORES', Astronomical & Astrophysical Transactions, 22:1, 33 - 41
To link to this article: DOI: 10.1080/1055679021000017448
URL: http://dx.doi.org/10.1080/1055679021000017448

Astronomical and Astrophysical Transactions,
2003, Vol. 22(1), pp. 33–41

HC_3N OBSERVATIONS OF THE OUTER GALAXY DENSE CORES

L. E. PIROGOV[a,*], L. E. B. JOHANSSON[b] and I. I. ZINCHENKO[a,c]

[a]*Institute of Applied Physics, Uljanova str., 46, Nizhny Novgorod, 603950, Russia;* [b]*Onsala Space Observatory, S-439 92, Onsala, Sweden;* [c]*Helsinki University Observatory, Finland*

(Received 9 April 2002)

Results of HC_3N observations of 15 dense molecular cloud cores, associated with bright IRAS sources in the outer Galaxy, are reported. HC_3N column densities and emission region sizes have been calculated. The $J = 10-9$ line analysis have been performed, along with the $J = 12-11$ and $J = 5-4$ data in the framework of the microturbulent isothermal model. The logarithms of densities found for 4 objects lie in the range: 5.5–5.9 being $\sim$(0.5–1) orders of magnitude higher than mean densities. Possible models for these objects should incorporate inhomogeneous density structure.

Keywords: Interstellar clouds, molecules: HC_3N, infrared sources, modelling

1 INTRODUCTION

Systematic studies of star forming regions, in the lines of molecules with high dipole moments, provide important information about physical conditions in dense cores associated with new born stars and help to reveal general properties of a sample under study. In recent years, a sample of bright IRAS sources in the outer Galaxy associated with high-mass stars and star clusters has been investigated in the HCO^+, NH_3, HCN and CS lines (Schreyer *et al.*, 1996; Pirogov, 1999; Zinchenko *et al.*, 1998) with nearly the same spatial resolution ($\sim 1'$). These observations have yielded important information about temperatures, masses, mean densities and velocity dispersions in the cores studied.

It is well known, however, that there is a significant difference between mean densities and densities derived from multiline excitation analysis, which are 1–2 orders of magnitude higher in high-mass star forming regions (see *e.g.* Zinchenko *et al.*, 1998). This fact indicates that emitting regions in many of these objects have inhomogeneous structure. To investigate further the density structure of the cores, one needs to perform multiline observations and analysis in lines of various density tracers.

For that purpose, the HC_3N molecule has been chosen. Due to its high dipole moment (3.7 D), the HC_3N molecule is an indicator of denser gas than many other high density tracers, including CS (2–1). Comparing with other molecules, HC_3N has important advantages, namely, large number of rotational transitions in the millimeter band and low optical depth

* Corresponding author.

ISSN 1055-6796 print; ISSN 1476-3540 online
DOI: 10.1080/1055679021000017448

of these transitions (Vanden Bout *et al.*, 1983, Bergin *et al.*, 1996). Observations of several selected massive star forming regions show than HC_3N lines are rather strong and can be readily detected with modern single dish telescopes (Vanden Bout *et al.*, 1983, Bergin *et al.*, 1996).

In order to get reliable density estimates in dense cores, associated with bright IRAS sources in the outer Galaxy, we have chosen three HC_3N transitions ($J = 5-4$, $J = 10-9$ and $J = 12-11$). Fifteen sources from full sample of IRAS sources with most intense HCN lines (≥ 2 K) (Pirogov, 1999) have been selected.

2 OBSERVATIONS

Observations have been performed in May–June 2001 at the 20-m OSO ratio telescope. Line and telescope parameters, as well as critical densities for each HC_3N transition, are given in Table I. The grid spacing for mapping was 20″. The $J = 5-4$ line was observed only toward $J = 10-9$ and/or $J = 12-11$ peaks.

Coordinates of the observed sources are given in Table II. This table also contains distances taken from Pirogov (1999) (see references therein), kinetic temperatures (from Schreyer *et al.* (1996)) based on ammonia observations and logarithms of mean densities (from Zinchenko *et al.*, 1998). The names of associated objects are also given in the table.

3 RESULTS

The HC_3N(10–9 and 12–11) have been detected in all sources. Three examples of integrated intensity maps are given in Figure 1. Integrated intensity distributions are very compact and

TABLE I Line and Telescope Parameters.

Transition	*ν (GHz)*	n_{cr} (cm^{-3}) $T_{kin} = 40$ K	*Beam width*	$\langle\eta_{MB}\rangle$	T_{sys} *(K)*	δV *(km/s)*
5–4	45.490	7.2×10^4	83″	0.7	170–300	0.08
10–9	90.979	6.2×10^5	42″	0.55	300–500	0.82
12–11	109.174	1.0×10^6	35″	0.45	400–700	0.69

TABLE II The Source List.

IRAS source	*α(1950)* (^{h}) (^{m}) (^{s})	*δ(1950)* (°)(′)(″)	*Distance (kpc)*	T_{kin}*(K)*	$\log \bar{n}$	*Associated objects*
00338+6312	00 33 53.3	63 12 32	0.85	25.6	5.0	RNO1b, L1287, G121.30
00494+5617	00 49 27.8	56 17 28	3.5	25.5		NGC281, S184, G123.07
02219+6152	02 21 55.3	61 52 34	2.3	30.0		W3-IRS5, S190, G133.71
02232+6138	02 23 13.7	61 38 46	2.3	32.3	4.9	W3(OH), G133.95
02575+6017	02 57 35.6	60 17 22	2.2	27.9		IC1848, S199
03035+5819	03 03 33.2	58 19 21	3.0	31.3	3.5	BFS26, G139.91
05274+3345	05 27 27.6	33 45 37	1.8	24.8		AFGL5142
05358+3543	05 35 48.8	35 43 41	1.8	25.1	4.2	S231
05375+3540	05 37 32.1	35 40 45	1.8	30.0	4.5	S235B, BFS46, G173.72
05377+3548	05 37 46.7	35 48 25	1.8	16.2		S235
05480+2545	05 48 04.8	25 45 29	2.1	19.8		BFS48
06056+2131	06 05 40.9	21 31 32	2.0	26.0		S247
06058+2138	06 05 53.9	21 38 57	2.0	26.3	4.3	S247, G188.95
06099+1800	06 09 57.9	18 00 12	2.5	30.8		S255
06384+0932	06 38 26.2	09 32 25	0.8	25.6	4.4	NGC2264, S273, G203.32

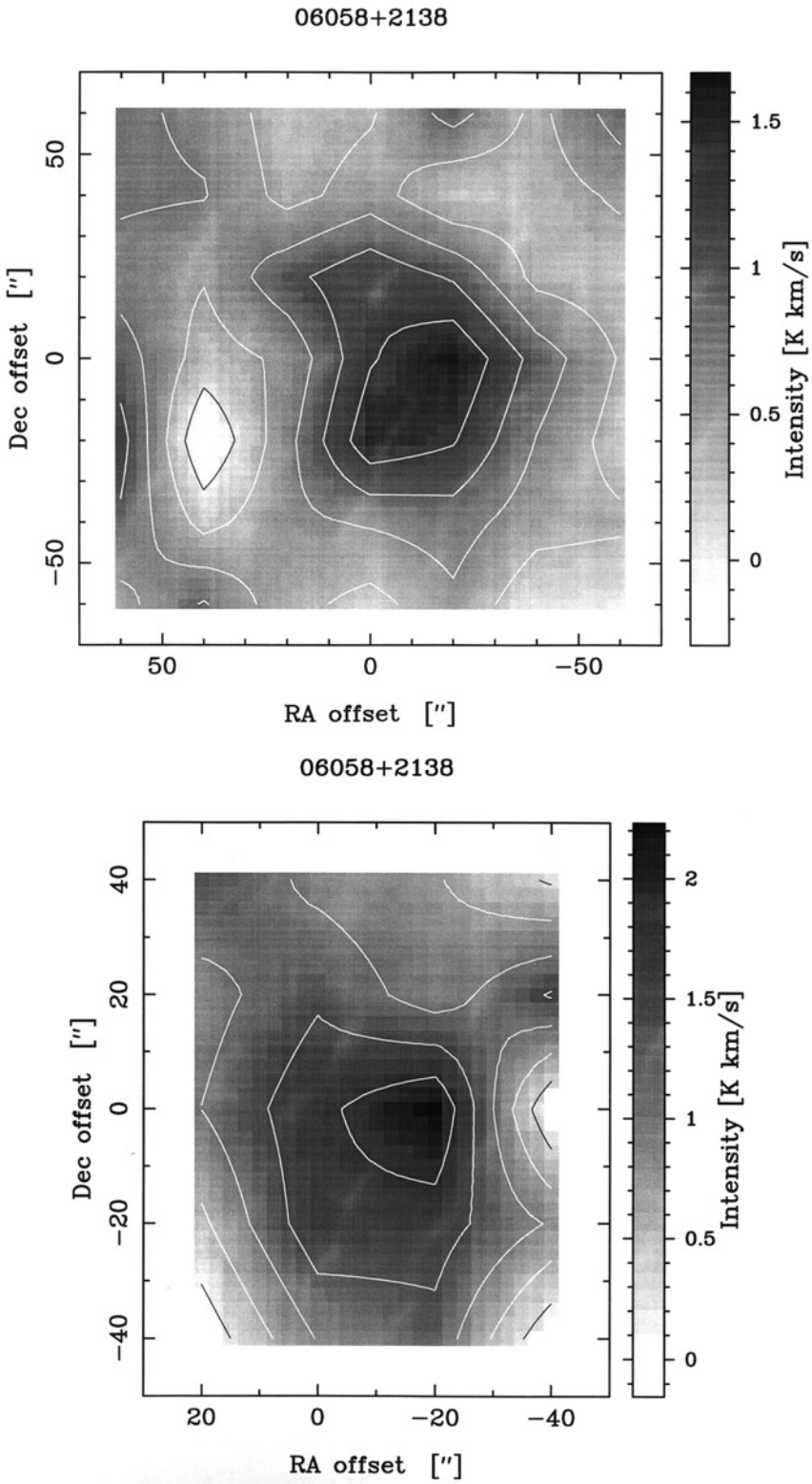

FIGURE 1 The $J = 10-9$ (upper panels) and $J = 12-11$ (lower panels) maps in three sample objects.

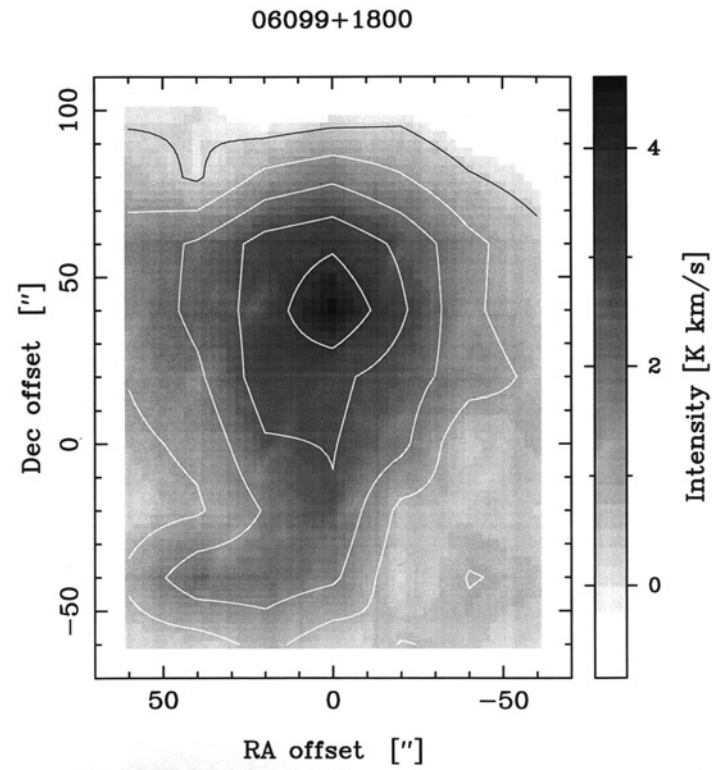

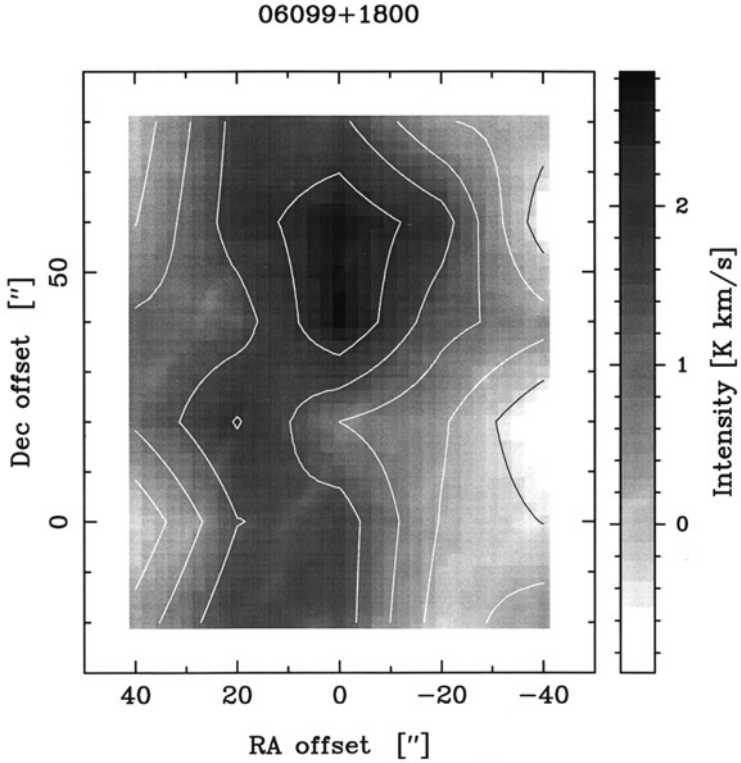

FIGURE 1 *(Continued)*

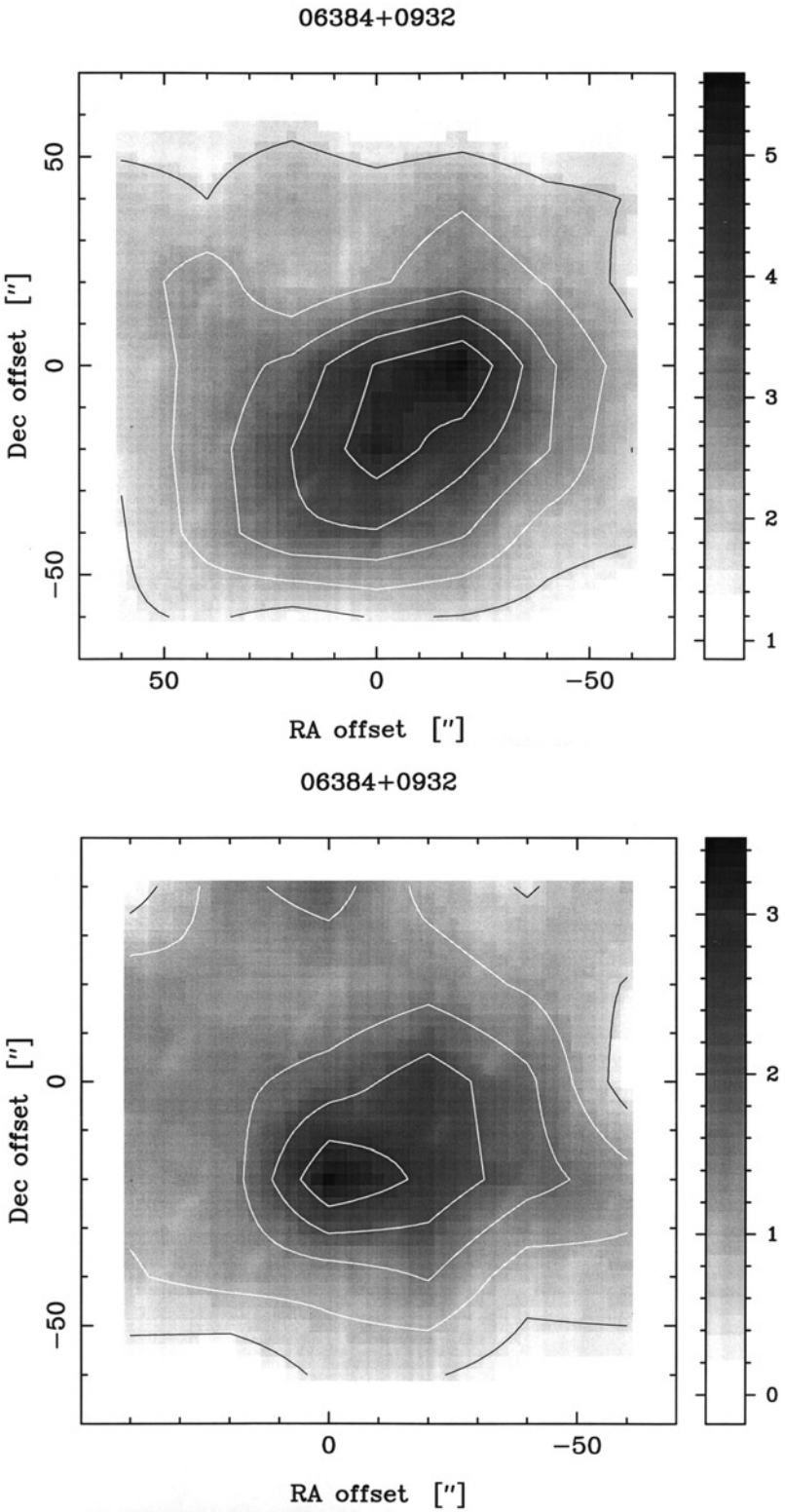

FIGURE 1 *(Continued)*

TABLE III The HC_3N(10–9) Peak Line Parameters, Emission Region Sizes and LTE Column Densities.

Source, position	*I(K km/s)*	T_{MB}*(K)*	V_{LSR} *(km/s)*	ΔV*(km/s)*	$\Delta\ominus(''$)	*d(pc)*	$N_{LTE}(cm^{-2})$
00338 + 6312(0, 0)	5.4(0.3)	2.0(0.1)	−17.66(0.04)	2.5(0.1)	25(2)	0.10(0.01)	$2.6\ 10^{13}$
00494 + 5617(0, 0)	4.2(0.5)	1.2(0.1)	−31.01(0.12)	3.3(0.2)	15(2)	0.26(0.03)	$2.0\ 10^{13}$
02219 + 6152(−20, 20)	3.5(0.4)	0.5(0.4)	−42.85(0.53)	7.8(1.3)	71(6)	0.79(0.07)	$1.6\ 10^{13}$
02232 + 6138(20, 0)	6.0(0.8)	2.3(0.2)	−47.21(0.12)	2.9(0.3)	22(2)	0.25(0.02)	$2.8\ 10^{13}$
02575 + 6017(−20, 20)	3.1(0.8)	0.8(0.2)	−38.23(0.39)	4.2(0.6)	62(7)	0.66(0.08)	$1.4\ 10^{13}$
03035 + 5819(−20, −20)	2.8(0.5)	0.5(0.1)	−40.65(0.59)	5.0(1.4)			$1.3\ 10^{13}$
05274 + 3345(20, 0)	3.7(0.3)	1.4(0.1)	−3.04(0.06)	2.5(0.1)	19(1)	0.17(0.01)	$1.8\ 10^{13}$
05358 + 3543(20, 20)	7.8(0.9)	2.0(0.2)	−16.77(0.14)	3.3(0.3)	14(1)	0.12(0.01)	$3.7\ 10^{13}$
05375 + 3540(0, −40)	3.6(0.4)	1.4(0.1)	−16.83(0.11)	2.7(0.3)	57(10)	0.50(0.09)	$1.7\ 10^{13}$
05377 + 3548(0, −40)	1.5(0.5)	0.8(0.2)	−19.88(0.18)	1.7(0.5)	105(8)	0.92(0.07)	$0.7\ 10^{13}$
05480 + 2545(0, −20)	4.8(0.5)	1.9(0.1)	−9.33(0.07)	2.3(0.2)	18(1)	0.18(0.01)	$2.3\ 10^{13}$
06056 + 2131(−20, 0)	4.7(0.3)	2.0(0.1)	2.37(0.05)	2.2(0.1)	24(2)	0.23(0.02)	$2.2\ 10^{13}$
06058 + 2138(−20, 0)	3.3(0.5)	1.5(0.1)	2.95(0.11)	2.2(0.3)			$1.6\ 10^{13}$
06099 + 1800(0, 40)	9.4(0.7)	2.3(0.1)	7.76(0.10)	3.8(0.2)	67(7)	0.81(0.09)	$4.4\ 10^{13}$
06384 + 0932(0, −20)	12.4(0.5)	4.2(0.1)	8.10(0.04)	2.6(0.1)	74(3)	0.29(0.01)	$5.8\ 10^{13}$

close to spherical symmetry (with the only exception of 06099 + 1800). The $J = 5-4$ line has been detected in thirteen sources (with signal-to-noise ratio > 5). As a rule, the $J = 10-9$ line is the most intensive one.

The HC_3N(10–9) integrated intensities, peak line temperatures, velocities and line widths obtained from Gaussian fits are given in Table III.

Emission region sizes (at half maximum intensity level) were obtained from fitting integrated intensity maps by 2D symmetric Gaussian function, taking emission region size and telescope beam width in quadrature. For two sources, fitting did not converge. Angular and linear sizes (d) for the $J = 10-9$ transition are given in Table III. The latter vary from 0.1 to 0.8 pc. The comparison with N_2H^+(1–0) (Pirogov *et al.*, 2002) and CS(2–1) (Zinchenko *et al.*, 1998) sizes for several sample objects shows that the HC_3N(10–9) regions are more compact and symmetric than the regions emitting in the lines of these density tracers.

HC_3N column densities, given in the last column of Table III, have been calculated using the $J = 10-9$ integrated intensities under LTE assumption, taking excitation temperature of 20 K, the value at which the estimate of the HC_3N column density is close to minimum.

4 MODEL ESTIMATES OF DENSITIES

Taking into account intensities of different HC_3N lines and kinetic temperatures of the cores, one could perform model calculations to derive densities. Since the spatial resolution at the $J = 5-4$ frequency is about two times worse than at the $J = 10-9$ and $J = 12-11$ frequencies, we performed 2D-Gaussian fitting of peak line temperatures distributions, followed by convolution with telescope beam at the $J = 5-4$ frequency (83″). The values of the convolved $J = 10-9$ and $J = 12-11$ line temperatures (T_c), as well as the ratios of these temperatures to the $J = 5-4$ line temperatures, are given in Table IV.

We performed calculations of HC_3N excitation in spherically-symmetric microturbulent cloud model with the power law radial dependence of density: $n(r) \propto n_0 r^{-\alpha}$. The calculations method was taken from Turner *et al.* (1997), adapted for HC_3N modeling. Model cloud consisted of 10 layers—within each of them density was constant. HC_3N–He collisional rates tabulated for distinct values of kinetic temperatures were taken from Green and Chapman (1978). We considered the cases $T_{KIN} = 20$ K and 40 K, the values which are the closest ones to the kinetic temperatures of the sample sources. It was found, however, that the model with $T_{KIN} = 20$ K fails to reproduce intensity ratios. Therefore, the following calculations were done for $T_{KIN} = 40$ K. In total, 15 HC_3N transitions were taken into account.

We considered the models with $\alpha = 0$, 1, 2 and microturbulent velocity, $V_{TURB} = 1$ km/s; 3 km/s. The results of calculations for the model with $\alpha = 0$ (homogeneous sphere) and

TABLE IV The HC_3N $J = 10-9$ and $J = 12-11$ Convolved Line Temperatures, Line Ratios and Logarithms of Model Densities.

Source, position	$T_c(10-9)$ *(K)*	$T_c(12-11)$ *(K)*	$T_c(10-9)/T(5-4)$	$T_c(12-11)/T(5-4)$	$\log n(H_2)$
00338 + 6312(0, 0)	0.96(0.19)	0.63(0.15)	2.6(6)	1.7(4)	5.5–5.7
02232 + 6138(20, 0)	1.18(0.29)	0.87(0.16)	3.0(7)	2.2(4)	5.85–5.9
05358 + 3543(20, 20)		0.71(0.14)		1.7(3)	5.6–6.1
05375 + 3540(0, −40)	0.66(0.16)		2.4(6)		≥ 5.25
05480 + 2545(0, −20)	0.64(0.20)		1.9(6)		≥ 5
06056 + 2131(−20, 0)	0.91(0.29)		1.7(6)		5–6.1
06099 + 1800(0, 40)	1.39(0.22)	0.69(0.21)	2.9(5)	1.4(4)	5.45–5.55
06384 + 0932(0, −20)	2.21(0.15)	1.45(0.14)	2.4(2)	1.6(2)	5.75

$V_{TURB} = 1$ km/s are shown in Figure 2, as the lines of constant $T(10-9)/T(5-4)$ ratio and constant $J = 10-9$ line temperatures versus HC_3N column densities (N) and density (n_0). Intensity ratios are shown by dashed-dotted lines, while line temperatures are shown by solid lines.

Using the diagram shown in Figure 2, we have calculated the ranges of N and n_0 for each of the considered sources. Combining together these results and those from the $J = 12-11$ and $J = 5-4$ data analysis, we have obtained the resulted ranges of densities, which are given in Table IV. The values of $\log(n_0)$ for 4 sources, where both $T(10-9)/T(5-4)$ and $T(12-11)/T(5-4)$ ratios are defined, vary in the range 5.5–5.9. This is $\sim$0.5–1 order of magnitude higher than mean densities from Table II, implying an existence of density inhomogenities of the cores. As the models with $\alpha = 1$, 2 give higher n_0 we consider the obtained values to be lower limits on densities within given spatial extent. It has been found that density estimates are insensitive to the value of turbulent velocity.

Calculated column densities for the model with $V_{TURB} = 3$ km/s are about half an order of magnitude higher than for the model with $V_{TURB} = 1$ km/s becoming, thus, closer to the LTE

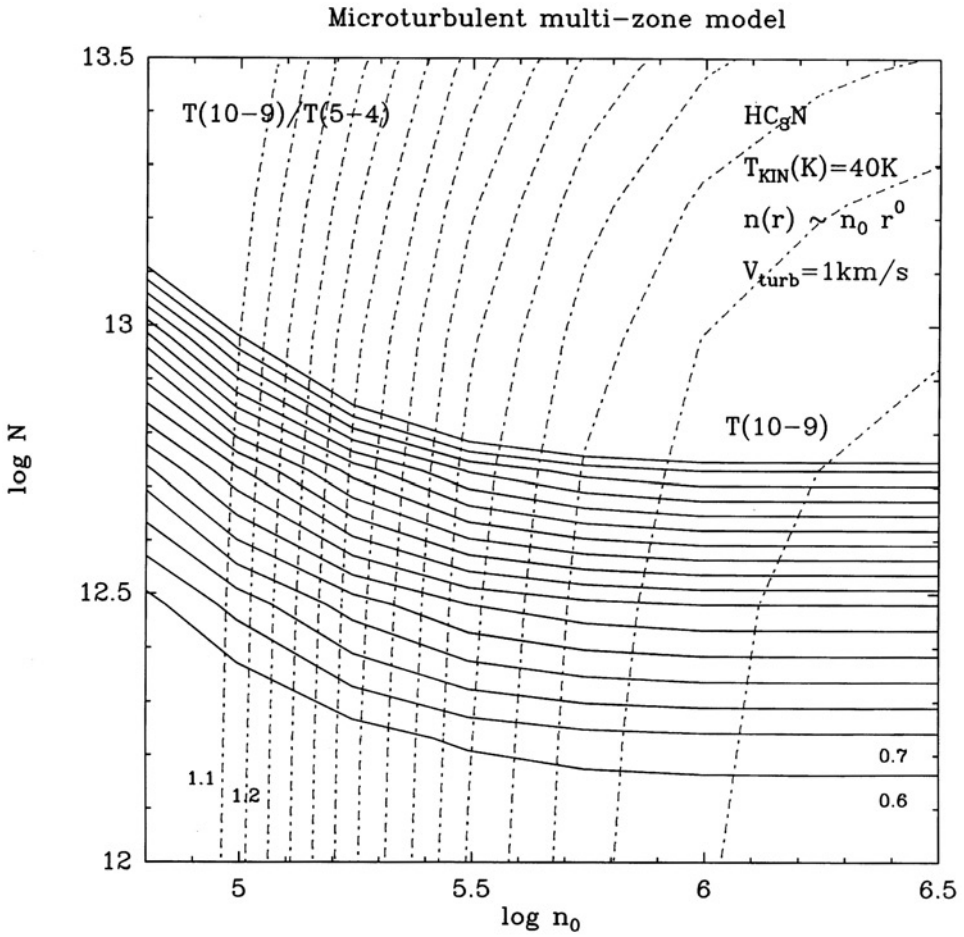

FIGURE 2 The results of calculations in the framework of the multi-zone microturbulent isothermal cloud model. The lines of constant $T(10-9)/T(5-4)$ ratio and $T(10-9)$ temperatures are plotted versus HC_3N column densities (N) and density (n_0). Intensity ratios are plotted by dotted-dashed curves beginning from 1.1 with 0.1 step; the $J = 10-9$ temperatures are plotted by solid curves beginning from 0.6 K with 0.1 K step.

values calculated in the previous section. Calculations also show that non-LTE effects are very strong in HC_3N excitation. Hence, the LTE approximation should be used with caution for estimates of total column densities in the sample objects.

5 CONCLUSIONS

In order to derive densities in fifteen dense molecular cloud cores associated with bright IRAS sources in the outer Galaxy multiline, HC_3N observations ($J = 5-4$, $J = 10-9$ and $J = 12-11$) have been performed.

The $J = 10-9$ emission region sizes at half maximum intensity level for thirteen sources lie in the range—0.1–0.8 pc. The HC_3N column densities obtained in the LTE approximation lie in the range—$(0.7–5.8) \cdot 10^{13}\,\mathrm{cm}^{-2}$.

Model calculations in the framework of the multi-zone isothermal microturbulent sphere have been performed. The $J = 10-9$ data have been analysed, along with the $J = 12-11$ and $J = 5-4$ data. As a result, the densities of several cores have been estimated. For four objects, the logarithms of densities lie in the range—5.5–5.9 being ~ 0.5–1 orders of magnitude higher than mean densities. Apparently, possible models for these objects should incorporate inhomogeneous density structure.

Acknowledgements

The work was supported by Russian Foundation for Basic Research grant 99-02-16556, INTAS grant 99-1667 and NASA-CRDF grant RPO-841.

References

Bergin, E. A., Snell, R. L. and Goldsmith, P. F. (1996). *Astrophys. J.*, **460**, 343.
Green, S. and Chapman, S. (1978). *Astrophys. J. Suppl.*, **37**, 169.
Pirogov, L. (1999). *Astron. Astrophys.*, **348**, 600.
Pirogov, L., Zinchenko, I., Caselli, P., Johansson, L. E. B. and Myers, P. (2002) (in preparation).
Schreyer, K., Henning, Th., Kömpe, C. and Harjumpää, P. (1996). *Astron. Astrophys.*, **306**, 267.
Turner, B. E., Pirogov, L. and Minh, Y. C. (1997). *Astrophys. J.*, **483**, 235.
Vanden Bout, P. A., Loren, R. B., Snell, R. L. and Wotten, A. (1983). *Astrophys. J.*, **271**, 161.
Zinchenko, I., Pirogov, L., Toriseva, M. (1998). *Astron. Astrophys. Suppl.*, **133**, 337.